

Comparing Compositions of Modern Cast Bronze Sculptures: Optical Emission Spectroscopy Versus x-Ray Fluorescence Spectroscopy

M.L. YOUNG^{1,3} and D.C. DUNAND²

1.—Department of Materials Science and Engineering, University of North Texas, Denton, TX 76203, USA. 2.—Department of Materials Science and Engineering, Northwestern University, Evanston, IL 60208, USA. 3.—e-mail: marcus.young@unt.edu

Bulk elemental compositions of 74 modern cast bronze sculptures from the collection at the Art Institute of Chicago, the Philadelphia Museum of Art, and the Rodin Museum (Philadelphia, PA) were determined using inductively coupled plasma-optical emission spectroscopy (ICP-OES) and a handheld x-ray fluorescence (XRF) spectrometer. The elemental compositions of the cast sculptures as measured previously by ICP-OES and presently by XRF are compared: A good match is found between the two methods for the base metal (Cu) and the two majority alloying elements (Zn and Sn). For both ICP-OES and XRF data, when the Zn composition is plotted versus the Sn composition, three discernable clusters are found that are related to the artist, foundry, casting date, and casting method; they consist of (A) high-zinc brass, (B) low-zinc, low-tin brass, and (C) low-zinc, tin bronze. Thus, our study confirms that the relatively fast, nondestructive XRF spectrometry can be used effectively over slower and invasive, but more accurate, ICP-OES to help determine a sculpture's artist, foundry, date of creation, date of casting, and casting method.

INTRODUCTION

While inductively coupled plasma (ICP) spectroscopy,^{1–10} x-ray fluorescence (XRF) spectroscopy,^{11–16} and scanning electron microscopy/energy-dispersive x-ray spectroscopy (SEM/EDX)^{12,17–22} have been used extensively and effectively to study archaeological metal sculptures, only a small number of studies have examined modern artistic metal sculptures using ICP spectroscopy,^{1,2,10,21} XRF spectroscopy,^{1,12,13,15} or SEM/EDX.^{12,20,21} The metal composition of 62 important modern bronze sculptures from the Art Institute of Chicago (AIC) and the Philadelphia Museum of Art (PMA) were measured by ICP-optical emission spectroscopy (OES) and provided a detailed picture of casting alloys employed at Parisian art foundries in the first half of the twentieth century.¹⁰ Sculpture compositions were correlated to the artist, foundry, casting date, and casting method. The goal of the current study is twofold: (i) to measure compositions on the same 62 modern bronze sculptures

using relatively rapid, nondestructive XRF and compare them with our previous ICP-OES results¹⁰ and (ii) to present compositional data collected by XRF on 12 additional modern bronze sculptures from the Rodin Museum (RM) in Philadelphia and discuss their correlations to the artist, foundry, date, and casting method in the context of the previously reported 62 modern bronze sculptures.

EXPERIMENTAL PROCEDURES

ICP-OES was performed at the Analytical Services Laboratory at Northwestern University using a Varian model ICP spectrometer as described in detail by Young et al.¹⁰ Quantitative XRF was performed on all 72 modern bronzes (Table I), as well as eight commercially available bronze standards and reference materials (for specific compositions, see Young et al.¹⁰) for calibration purposes, using a portable XRF device (KeyMaster's TRACeR III) with a Rh anode and an Al filter, which was operated at 40 kV and 1 mA for 60 s. The beam size is

Table I. Description of the 74 modern bronzes (62 previously studied by ICP-OES¹⁰) studied here using XRF including artist, accession number, title, and method of analysis

Artist	Accession Number	Title	XRF	ICP-OES
Bernard	AIC: 1943.1189a	Girl with Pail	X	X
Bonnard	AIC: 1963.927a	Spring Frolic	X	X
Bouraine	AIC: 1973.774c	Dancing Woman with Hoop	X	X
Bourdelle	AIC: 1997.543a	Head of Apollo	X	X*
	AIC: 1950.141a	Head of Young Woman	X	X
	AIC: 1925.255a	Heracles (Archer)	X	X*
	AIC: 1953.168	Penelope	X	X
Brancusi	PMA: 1967.30.6a, b	Danaide	X	X
	AIC: 1990.88	Golden Bird	X	
	AIC: 1930.523	Sleeping Muse	X	
	AIC: 1985.542a, b	Suffering	X	X*
Darde	AIC: 1950.143	Sorrow	X	
Daumier	PMA: 1957.127.11a, b	Alexandre-Simon Pataille	X	X
	PMA: 1986.26.275a	L'Obsequieux	X	X
	PMA: 1986.26.9a, b	Ratapoil	X	X
Degas	PMA: 1950.92.39	Rearing Horse	X	
	PMA: 1954.92.21a, b	Torso/Woman Rubbing her Back with a Sponge	X	X
	PMA: 1963.181.82a, b	Woman Taken Unawares	X	X
Derain	AIC: 1978.410	Man with Large Ears	X	
Despiau	AIC: 1954.324	Madame De Waroquier	X	X
	AIC: 1950.93a	Young Girl	X	X
Drappier	AIC: 1984.164	Stray Horse	X [†]	
Duchamp-Villon	AIC: 1957.165a	Horse	X	X
	AIC: 1963.371	Portrait of Dr. Gosset	X	
Knoop	AIC: 1939.238a	Kathleen Cornell	X	X
Landowski	AIC: 1923.314	Henry Harrison Getty	X	X
Lipchitz	AIC: 1996.394	Mother and Child	X	X
	AIC: 1943.594a	Rape of Europa	X	X
	AIC: 1955.826	The Reader	X	X
	PMA: 1949.78.1a, b	Sailor with Guitar	X	X
	PMA: 1955.96.2a, b	Woman with Braid	X	X
Maillol	AIC: 1955.29	Enchained Action	X	
	AIC: 1934.383a	Girl with Arm over Eyes	X	X
	AIC: 1947.86a	Leda	X	X
	PMA: 1950.92.44a	Leda	X	X
	AIC: 1934.384a	Nude	X	X
	AIC: 1932.1144	Renoir	X	X
	AIC: 1971.779a	Woman with Crab	X	X
Matisse	AIC: 1958.16a	Seated Nude	X	X
	PMA: 1960.146.1a, b	Seated Nude with Pedestal	X	X
	AIC: 1949.202a, b	The Serf	X	X
	PMA: 1963.210a, b	Serpentine Woman	X	X
	PMA: 1967.030.51a, b	Standing Nude with Arms Raised	X	X
	AIC: 1992.654a	Woman Leaning on Her Hands	X	X
	AIC: 1932.1145	Woman without Arms	X	X
Orloff	AIC: 1930.227a	Woman with Basket	X	X
Picasso	AIC: 1967.682b	Female Figure	X	X
	AIC: 1957.70a, b	Flowers in a Vase	X	X*
	AIC: 1949.584	Head of a Woman (Fernande)	X	X
	AIC: 1964.193	Jester	X	X
	AIC: 1967.683	Standing Woman 1	X	X
	AIC: 1967.685b	Standing Woman 2	X	X
	AIC: 1967.686	Standing Woman 3	X	X
	AIC: 1967.687	Standing Woman 4	X	X
	AIC: 1967.688	Standing Woman 5	X	X
	AIC: 1967.689	Standing Woman 6	X	X
	AIC: 1967.690	Standing Woman 7	X	X
	AIC: 1967.684	Standing Woman 8	X	X

Table I. continued

Artist	Accession Number	Title	XRF	ICP-OES
Poupelet	AIC: 1927.366	Cat	X	X
	AIC: 1931.569	Cat	X	X
	AIC: 1927.368a	Cock	X	X
	AIC: 1927.365.2	Cow	X	X
	AIC: 1931.568a	Goat	X	X
	AIC: 1927.369a	Goose	X	X
	AIC: 1927.365.1	Peasant	X	X
	AIC: 1927.367a	Rabbit	X	X
	AIC: 1925.726	Woman at Her Toilet	X	
	AIC: 1927.364	Woman Bathing	X	X
Renoir	PMA: 1950.92.47a,b	Head of Coco	X	X
Rodin	PMA: 1967.30.73a,b	The Athlete	X	X
	PMA: 1929.7.4a,b	The Athlete	X	X
Zadkine	RM: 1929.7.123	The Thinker	X	
	RM: 1929.7.128	Gates of Hell	X	
	PMA: 1964.80.1a, b	Harlequin	X	X

More details can be found in Young et al.¹⁰*ICP-MS was also performed.†Only patina was measured.

elliptical in shape with a ~6 mm minor axis and a ~7 mm major axis. Elemental compositions were determined using one of the Cu-based empirical quantification methods database provided by KeyMaster (now Bruker, Billerica, MD). XRF spectra were collected from areas with little or no patina, often near sites scraped and drilled for ICP-OES sample collection. Although the measurements were performed in air, the XRF spectrometer was placed as close to the sample as possible and in areas where the surface was as flat as possible to minimize errors in the measurement. As illustrated in Fig. 1b, these sites were generally collected under the base of the sculpture where removal of material for ICP-OES would not be noticeable during sculpture display. The green box in Fig. 1b highlights the location of an example site where ICP-OES and XRF measurements were collected. Figure 1c shows a detailed view of this example site (red oval) where ICP-OES and XRF measurements were collected. In the case of Brancusi's *Suffering* (AIC: 1985.542), ICP-OES samples were scraped from the bottom of the sculpture and then XRF measurements were performed on this same location of the sculpture (red oval in Fig. 1c).

In our XRF study, generally only one location was selected for analysis. Variations in composition are expected depending on sampling location;²³ however, for many of the bronze sculptures in this study, the distinguishing characteristic compositions are separated by several wt.%Zn and a few wt.%Sn, thus the sampling location is less critical. To illustrate this point, elemental compositions from two different sites (base and main body of the same sculpture) are shown for Matisse's *The Serf* (AIC: 1949.202a and b) and Picasso's *Flowers in a Vase* (AIC: 1957.70a and b). For both sculptures, the base and main body are believed to have been cast separately and welded together. Matisse's *The Serf* (AIC: 1949.202a and b) shows a difference of

less than 1 wt.%Zn and 1 wt.%Sn and Picasso's *Flowers in a Vase* (AIC: 1957.70a and b) shows a difference of less than 0.2 wt.%Zn and 1.5 wt.%Sn. In most cases, only one site was used for measurement. While this approach appears valid for comparisons where compositions are separated by several wt.%Zn and a few wt.%Sn as in this case, it is nevertheless recommended that multiple sites should be measured when possible. Furthermore, microscopic variations are expected due to the presence of various metallurgical phases, but the large beam size tends to average out these differences.^{18,23} It has been observed in Refs. 18, 19, 23 that the presence of Pb (which forms large insoluble globules in Cu) can lead to inhomogeneous microstructure and thus inhomogeneous measurements. In our study, most bronze sculptures have less than 1 wt.%Pb; due to this low concentration, Pb was not used to distinguish characteristic clusters for the bronze sculptures.

Although empirical methods for quantification provided by the XRF spectrometer manufacturer are known to be inaccurate for precise composition measurements of archaeological bronzes due to elemental depletion or enrichment at the surface (as a result of having often been subjected to centuries of corrosion), modern bronzes are known to be typically more accurate as the XRF instruments are designed for commercial use on modern alloys.^{23,24} In the current study, we used a calibration method based on the manufacturer's recommended Cu-based empirical quantification method. As mentioned above, eight commercially available bronze standards and reference materials (three of which more closely matched compositions of the bronze sculptures studied here—for specific compositions, see Young et al.¹⁰) were used for calibration purposes as well as to alleviate the issues associated with the empirical calibration. As reported previously,¹⁰ the standard deviation for averaged values of three

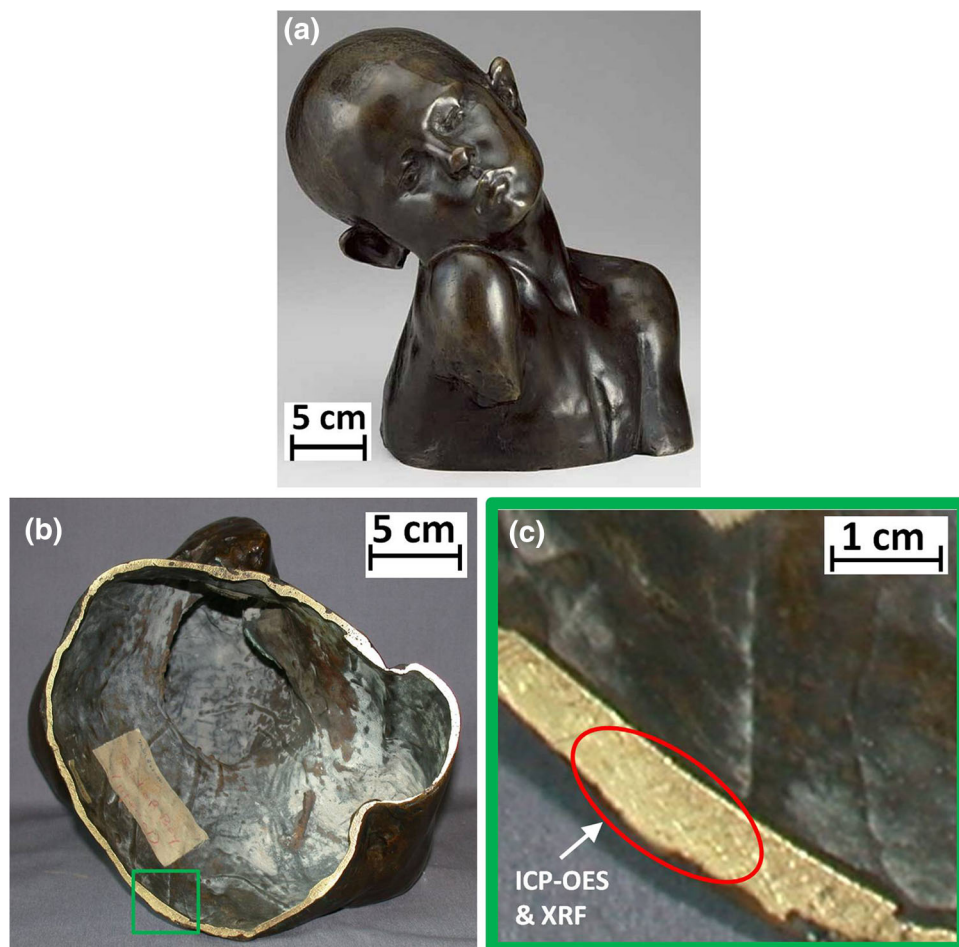


Fig. 1. (a) Photograph of Brancusi's bronze sculpture *Suffering*, which was created before 1907 and cast in 1907 using the lost wax process at the C. Valsuani foundry and is now in the Art Institute of Chicago's collection (AIC: 1985.542). (b) Photograph of the base of Brancusi's *Suffering*. Green box shows the location of an example site where ICP-OES and XRF measurements were collected. (c) Detailed view of an example site (red oval) where ICP-OES and XRF measurements were collected (Color figure online).

ICP-OES measurements were within 0.5 wt.% of any given element from standards and reference materials. Table II shows the elemental compositions determined by the manufacturer and measured by XRF of the three reference materials, which most closely matched the compositions of our bronze sculptures. Both the references and standards in Table II from National Institute of Standards and Technology (NIST) and SiPi Metals Corporation (SIPI) used methods that very accurately predict the composition. These calibration measurements provide credence that the measurements for the modern bronze sculptures are accurate. While eight total references and standards were used, only three are presented in Table II as they most closely match the compositions of the modern bronze sculptures in this study. For each reference material, three separate XRF measurements were collected and the average value is reported here. As illustrated in Table II, all averaged values of three XRF measurements from each bronze standards and reference materials were within 1 wt.% for each element of any given measurement reported by the manufacturer. The empirical quantification method also uses an interelement correction for overlapping

peaks and the data are normalized with special attention to Cu, as this is known to be the most sensitive element in bronzes.²³ The empirical quantification method was used to quantify eight elements (Cu, Zn, Sn, Pb, Fe, Ni, Mn, and Sb). Due to inaccuracies in the limits of detection and quantification, only the base metal (Cu) and majority alloying elements (Zn and Sn) were used for cluster identification, whereas the minority alloying element (Pb) and the impurity elements (Fe, Ni, Mn, and Sb) were not used. For future studies, it is recommended that a complementary method, such as SEM or ICP-OES, the latter being used here, is used to validate XRF measurements from, at a minimum, a few representative bronze sculptures.

RESULTS AND DISCUSSION

Table I provides a brief description of the 74 modern bronze sculptures studied here and designates whether XRF and/or ICP-OES measurements were collected for each individual sculpture. Details such as foundry, casting method, date of creation, and date of casting, as well as elemental compositions

Table II. Elemental compositions of three reference materials as reported by the manufacturers and measured by XRF for the base metal (Cu), majority alloying element (Zn and Sn), minority alloying element (Pb), and the main impurity elements (Fe and Ni)

Standards	Commercial name	Data source	Composition in (wt.%)						Absolute composition change (wt.%)					
			Cu	Zn	Sn	Pb	Fe	Ni	Between manufacturer and XRF					
			Cu	Zn	Sn	Pb	Fe	Ni	Cu	Zn	Sn	Pb	Fe	Ni
NIST C1107	Naval Brass	Manufacturer	61.21	37.34	1.04	0.18	0.037	0.098	0.26	0.67	0.07	0.00	0.03	0.03
		XRF	61.5	36.7	0.97	0.18	0.01	0.07						
SIPI C84400	Leaded Semi-Red Brass	Manufacturer	80.75	9.18	2.7	6.49	0.27	0.52	0.35	0.95	0.00	0.06	0.01	0.04
		XRF	80.4	8.2	2.70	6.43	0.26	0.56						
SIPI C83300	Contact Metal	Manufacturer	92.46	4.53	1.58	1.1	0.11	0.19	0.99	0.50	0.09	0.15	0.02	0.05
		XRF	91.5	4.0	1.67	1.25	0.13	0.14						

Table III. Description of the additional 12 modern bronzes studied by XRF only, including artist, accession number (AIC, PMA, and RM indicate the sculpture is from the collection of The Art Institute of Chicago, the Philadelphia Museum of Art, or the Rodin Museum, respectively), title, foundry, casting method, date of creation, date of casting, and corresponding cluster (A, B, C, and O for outliers)

Artist	Accession number	Title	Foundry	Casting method	Creation date	Casting date	Cluster
Brancusi	AIC: 1990.88	Golden Bird		Lost wax	1919–1920		O
	AIC: 1931.523	Sleeping Muse	C. Valsuani	Lost wax		1910–1913	A
Darde	AIC: 1950.143	Sorrow	Alexis Rudier	Sand	1916		C
Degas	PMA: 1950.92.39	Rearing Horse	Hébrard	Lost wax	Post-1920		A
Derain	AIC: 1978.410	Man with Large Ears			(1938–1953)		B
Drappier	AIC: 1984.164	Stray Horse	Siot-Decauville		1906		O
Duchamp-Villon	AIC: 1963.371	Portrait of Dr. Gosset	Georges Rudier		1957		A
Maillol	AIC: 1955.29	Enchained Action	Rudier	Sand	(c. 1909)		C
Picasso	AIC: 1967.684	Standing Woman 8					A
Poupelet	AIC: 1925.726	Woman at Her Toilet		Sand	(Pre-1907)		B
Rodin	RM: 1929.7.123	The Thinker	Alexis Rudier	Sand		1925	C
	RM: 1929.7.128	Gates of Hell	Alexis Rudier	Sand		1928	C

In the “Casting method” and “Creation date” columns, parentheses indicate value is likely (as inferred by visual observation and available information) but not known.

(wt.%) based on ICP-OES measurements for 62 of the sculptures, can be found in Young et al.¹⁰ For example, Fig. 1a shows a photograph of Constantin Brancusi’s bronze sculpture titled *Suffering*, which was created before 1907 and cast in 1907 using the lost-wax process at the C. Valsuani foundry, which is now in the AIC’s collection (Accession #1985.542). As shown in the abbreviated Table I, the previous ICP-OES study¹⁰ focused on modern bronze sculptures, many of which were cast in Parisian foundries in the first half of the twentieth century (from the 1900s to the 1950s) from 20 prominent artists of the time, including Brancusi, Daumier, Degas, Maillol, Matisse, Picasso, Poupelet, Renoir, and Rodin. In addition to the sculptures

studied by Young et al.,¹⁰ the current study presents data on nine new sculptures from artists included in the previous study (i.e., Brancusi’s *Golden Bird* and *Sleeping Muse*, Degas’ *Rearing Horse*, Duchamp-Villon’s *Portrait of Dr. Gosset*, Maillol’s *Enchained Action*, Picasso’s *Standing Woman 8*, Poupelet’s *Woman at Her Toilet*, and Rodin’s *The Thinker* and *Gates of Hell*) as well as three sculptures from artists of the same time period not included in the previous study (i.e., Darde’s *Sorrow*, Derain’s *Man with Large Ears*, and Drappier’s *Stray Horse*), as illustrated in Table III and the artist in bold print in Table IV. Table IV shows the elemental composition based on XRF measurements for the 74 modern bronzes from

Table IV. continued

Artist	Museum	Accession	XRF composition (wt.%)								Testing Surface	Absolute composition change (wt.%) between ICP-OES and XRF							
			Cu	Zn	Sn	Pb	Fe	Ni	Mn	Sb		Cu	Zn	Sn	Pb	Fe			
Matisse	AIC	1949.202b (figure)	91.8	3.9	1.73	0.9	0.16								0.70	0.16	0.22	0.25	0.02
Matisse	PMA	1967.030.51***	91.65	3.15	2.7	0.545	0.3								2.55	0.38	1.01	0.45	0.07
Matisse	AIC	1932.1145	90.5	3.7	2.8	1.59	0.22								2.30	0.16	0.67	0.63	0.08
Picasso	AIC	1967.682	88.4	5.8	2.7	1.7	0.14								1.50	0.41	0.38	0.35	0.09
Picasso	AIC	1964.193	91.7	5	1.27	0.33	0.08								1.30	0.78	0.26	0.26	0.05
Poupelet	AIC	1925.726	91.8	3.9	2.3	0.48	0.16												
Poupelet	AIC	1927.366	88.1	6.5	2.9	0.5	0.17												
Poupelet	AIC	1927.365.2	89.4	6.6	1.63	0.27	0.15								2.90	0.51	1.28	0.36	0.07
Poupelet	AIC	1931.568	92	4.4	1.16	0.5	0.16								1.40	0.51	0.17	0.11	0.16
Poupelet	AIC	1927.367	93.2	3.2	1.87	0.37	0.11								1.20	0.45	0.13	0.01	0.07
Poupelet	AIC	1927.364	91.7	4.6	1.7	0.47	0.09								0.69	0.75	0.13	0.09	0.05
Cluster C															1.70	0.07	0.06	0.13	0.03
Bourdelle	AIC	1997.543	90.4	0.98	6.1	0.47	0.55								4.61	0.20	2.15	0.38	0.53
Bourdelle	AIC	1950.141	91.1	1.49	4.2	0.49									4.00	0.07	1.01	0.41	0.07
Bourdelle	AIC	1925.255	92.8	0.92	4.2	0.8	0.32								2.40	0.14	0.52	0.78	0.32
Daumier	PMA	1986.26.9**	92.65	0.6	4.55	0.92	0.29								3.05	0.38	1.51	0.82	0.25
Darde	AIC	1950.143	92.1	1.25	3.9	1.42	0.32												
Maillol	AIC	1955.29	91.1	2.2	5.6	0.31	0.16												
Orloff	AIC	1930.227	93	1.47	4.3	0.24	0.18												
Poupelet	AIC	1927.368	93.2	1.5	3.8	0.63	0.17								2.00	0.15	0.82	0.19	0.14
Poupelet	AIC	1927.365.1	91.7	2.1	4.2	0.71	0.24								0.40	0.39	0.02	0.12	0.10
Rodin	PMA	1967.30.73	93.4	1.01	4.8	0.15	0.14								1.50	0.02	0.30	0.25	0.07
Rodin	PMA	1929.7.4	94.5	0.48	3.9	0.19	0.24								0.60	0.47	0.51	0.10	0.11
Rodin	RM	1929.7.123	93.2	0.83	5	0.1	0.19								0.60	0.26	0.06	0.08	0.22
Rodin	RM	1929.7.128	90.6	1.13	6.7	1.08	0.17												
Outliers																			
Bouraine	AIC	1973.774	74.4	22.3	0.21	0.32	0.1								3.50	1.90	0.24	0.55	0.10
Bourdelle	AIC	1953.168	87.2	7.5	3	0.61	0.1								1.77	0.60	0.30	0.46	0.10
Brancusi	AIC	1990.88***	68.5	27.1	1.2	1.14	0.26												
Daumier	PMA	1957.127.11	86.7	6.8	3	0.44	0.44								1.90	1.26	0.32	0.09	0.31
Daumier	PMA	1986.26.275	86.2	8.2	3.3	0.27	0.09								2.00	0.34	0.34	0.12	0.05
Drappier	AIC	1984.164	76.9	18.4	0.95	1	0.21												
Duchamp-Villon	AIC	1957.165	73.8	22.2	1.09	0.73	0.09								1.40	0.11	0.26	0.52	0.01
Landowski	AIC	1923.314	79.8	5.8	7.6	1.39	1.45								6.10	1.78	2.21	0.55	1.30
Lipchitz	AIC	1996.394	87.9	5	3.6	1.3	0.37								1.70	0.26	0.28	0.01	0.17
Lipchitz	AIC	1943.594	89	3.3	5.6	1.45	0.11								0.10	0.06	0.19	0.43	0.03
Lipchitz	AIC	1955.826	90.8	2	4.7	1.1	0.31								3.10	3.66	0.75	1.43	0.31
Lipchitz	PMA	1949.78.1***	85.3	6.1	6.3	0.56	0.24								1.50	0.19	0.03	0.22	0.06
Lipchitz	PMA	1955.96.2	85.2	7.9	4.4	0.48	0.16								0.55	0.95	0.34	0.17	0.04

Table IV. continued

Artist	Museum	Accession	XRF composition (wt.%)										Absolute composition change (wt.%) between				
			Cu	Zn	Sn	Pb	Fe	Ni	Mn	Sb	ICP-OES and XRF						
											Cu	Zn	Sn	Pb	Fe		
Lipchitz	PMA	1955.96.2**	84.4	7.8	5.5	0.66	0.19	0.02	0.07	Scraped	0.20	0.90	0.79	0.12	0.03		
Maillol	PMA	1950.92.44	92.6	2.2	3.1	0.35	0.28	0.04	0.11	Patina	0.10	0.96	0.34	0.23	1.04		
Picasso	AIC	1949.584	92.4	4.7	2.5	0.41	0.07	0.03	0.01	Scraped	0.90	1.70	2.44	0.14	0.03		
Poupelet	AIC	1931.569	61.1	34.4	0.73	3	0.3	0.03	0.01	Scraped	1.20	0.90	0.01	0.19	0.12		
Zadkine	PMA	1964.80.1a,b	81.6	13.7	0.99	0.8	0.2			Scraped	3.70	0.90	0.12	0.04	0.05		

In addition to the elemental composition, a description of the testing surface and the absolute difference in wt.% between ICP-OES and XRF measurements, when present, is also included. The additional 12 modern bronzes studied by XRF only are in bold print**. An average of two measurements***An average of three measurements, respectively

AIC, PMA, and RM, which are separated according to compositionally similar groups (clusters A, B, and C and outliers), as described in detail by Young et al.¹⁰

Comparison Between XRF and ICP-OES Compositional Data

Figure 2a–e shows a comparison from 62 bronze sculptures (listed in Table I and compared in Table IV) between ICP-OES and XRF measurements for Cu, Zn, Sn, Pb, and Fe concentrations, where a perfect correlation is represented by a black line with slope of unity. As illustrated in Fig. 1a and b, the Cu and Zn concentrations tend to be higher for ICP-OES by an average of 1.9 wt.% and 1.1 wt.%, respectively, compared with XRF. By contrast, the Sn, Pb, and Fe concentrations tend to be lower for ICP-OES by an average of 0.6 wt.%, 0.4 wt.%, and 0.2 wt.%, respectively, compared with XRF. A comparison between laser ablation ICP-MS and handheld XRF measurements for Sn and Zn concentrations (Fig. 1b and c) was previously reported by Dussubieux on 10 bronze sculptures from Matisse at the Baltimore Museum of Art.¹ They found that, compared with ICP, the handheld XRF overestimated the concentrations of both elements: by ~1 wt.% on average for Sn (for ICP compositions spanning 2–6 wt.%), and by ~3 wt.% on average for Zn (with ICP compositions spanning 3–13 wt.%).

Our previous ICP-OES results on 62 bronze sculptures revealed correlations based on the artist, foundry, casting method (sand or lost wax), and casting date.¹⁰ By plotting the ICP-OES concentrations of the two main alloying elements (Zn and Sn) against each other, three clusters became evident: (A) high-zinc brass, (B) low-zinc brass, and (C) tin bronze (as labeled in Fig. 4); outliers are also present. As illustrated in Fig. 3, a similar plot of Zn versus Sn composition for ICP-OES (solid symbols) and XRF (hollow symbols) shows the data divided into the three main clusters (A, B, and C). Although the three clusters determined from XRF data are shifted to higher Sn values (as expected from the trend visible in Fig. 1c), most data points from XRF can still be assigned to their original clusters, as determined by ICP-OES. Due to the reasonably large compositional variation between clusters, Fig. 3 confirms that XRF can be used effectively to help determine a sculpture’s artist, foundry, date of creation, date of casting, and casting method.

ICP-OES is a time-consuming, destructive method that requires removal of material (albeit in amounts as low as ~30 mg) and then dilutions with varying concentrations in an acid from these samples as well as reference samples. By contrast, XRF is completely nondestructive, making it more attractive for valuable, heavy, and/or fragile objects. For the same reason, the portability of the XRF instrument is a notable advantage. Furthermore, the time to perform an XRF measurement is much shorter: minutes to locate a spot representative of the bulk metal and to perform the analysis on site, compared with hours to drill, collect, transport, and dissolve the metallic shavings and

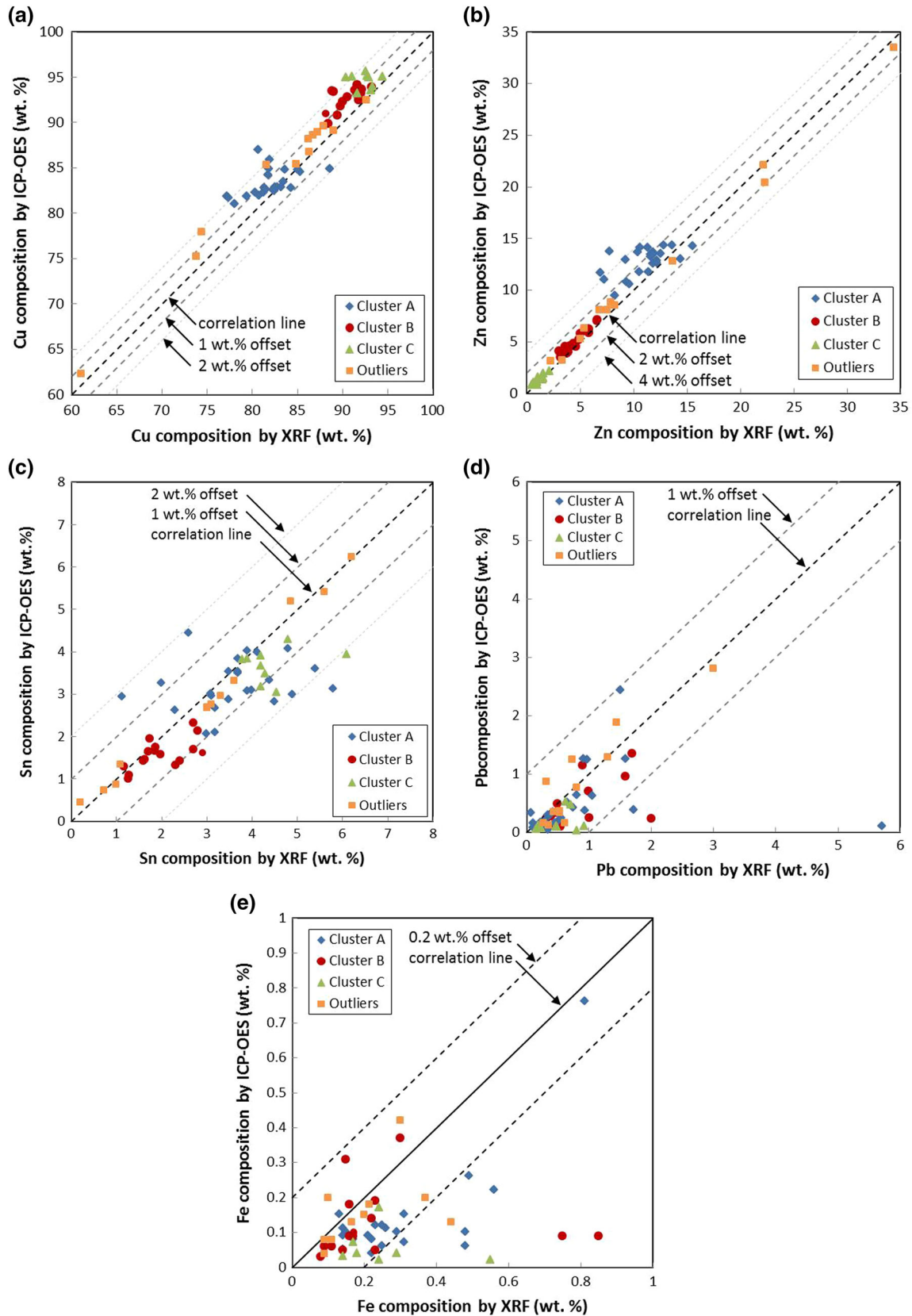


Fig. 2. Comparison between ICP-OES and XRF measurements for concentrations of the base metal (a) Cu, majority alloying elements (b) Zn, (c) Sn, minority alloying element (d) Pb, and main impurity element (e) Fe. Black line represents exact correlation and dotted lines represent a given \pm wt. % offset from the correlation line.

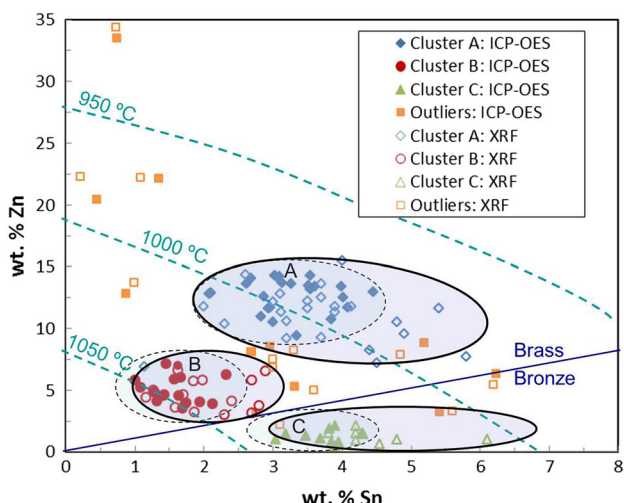


Fig. 3. Plots of Zn versus Sn concentrations measured via ICP-OES (solid symbols; data from Young et al.¹⁰) and XRF (hollow symbols). Clusters are indicated, as well as liquidus temperature of alloys.¹⁰ The 12 new bronze sculptures are not included in this figure as ICP-OES data was not collected for them.

perform the analysis off site. However, the larger spot size for the XRF measurement can make it difficult to target an area that is completely representative of the bulk metal (e.g., free of patina or corrosion layer); on the other hand, the very small area and volume sampled by ICP-OES make it more prone to error due to composition fluctuation in the sculpture (i.e., from segregation and local corrosion), necessitating additional measurements. Also, because the XRF is sampling the near surface rather than the bulk of the object, the measurements may not be representative of the bulk composition due to microstructural variations as a result of corrosion processes (e.g., dezincification) or elemental segregation on casting (the surface being first to solidify may be enriched or depleted in segregating elements). Similarly, ICP-OES samples are generally coming from the near surface (no more than a few millimeters into the sculpture) and may thus also be subjected to such errors. Although it is expected that both techniques become less accurate when measuring lower concentrations of minority alloying elements (e.g., Pb) and eventually main impurity elements (e.g., Fe), ICP-OES measurements have a higher degree of accuracy as compared to XRF measurements. In the case of the modern bronze sculptures studied here, however, the same overall conclusions can be deduced from measurements by either technique: Both XRF and ICP-OES measurements show the same clusters due to the reasonably large compositional variation existing between these clusters.

Classification of 12 Additional Modern Sculptures

Table III provides a brief description of the additional 12 modern bronzes studied by XRF only.

Figures 4, 5, 6a and b, and 7 show plots of Zn versus Sn concentrations based solely on XRF measurements

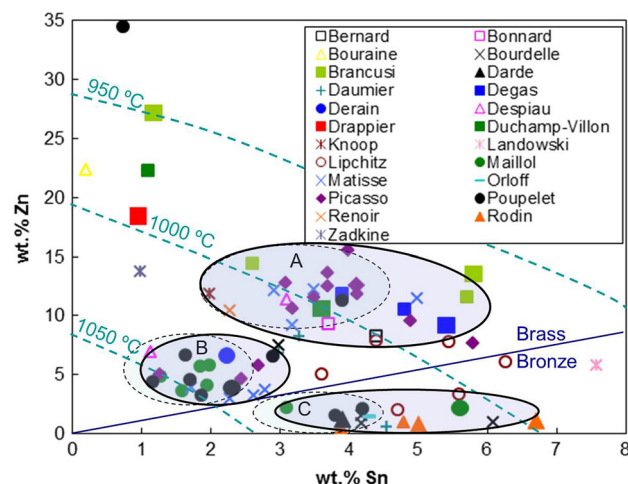


Fig. 4. Elemental composition plots (Zn versus Sn as determined by XRF) for sculptures identified by artist. The normal-sized symbols are from the current XRF data, which correlate with previous ICP-OES data,¹⁰ while the oversized symbols are from the current XRF data from the 12 sculptures not previously reported. The three ovals indicate alloy clusters (A, B, and C) from the previous ICP-OES study¹⁰ (dashed lines) and the current XRF study (solid lines).

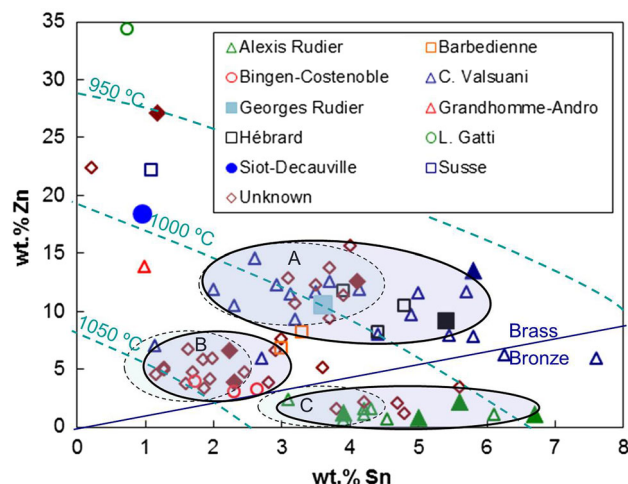


Fig. 5. Elemental composition plots (Zn versus Sn as determined by XRF) for sculptures identified by foundry. The open symbols are from the current XRF data which correlates previous ICP-OES data,¹⁰ whereas the solid symbols are from the current XRF data from the 12 sculptures not previously reported. The three ovals indicate alloy clusters (A, B, and C) from the previous ICP-OES study¹⁰ (dashed lines) and the current XRF study (solid lines).

for these 12 new pieces as well as the original 62,¹⁰ as identified by the artist, foundry, date of sculpture creation, casting date, and casting method, respectively. Data from the additional 12 sculptures do not invalidate the three clusters A–C (ovals with dashed lines, Figs. 4, 5, 6, and 7) based on the original 62 sculptures,¹⁰ but clusters A, B, and C are shifted to higher and broader Sn concentrations due to a systematic bias toward higher Sn concentrations as measured by XRF. To incorporate nearly all of the XRF data with these shifted values, clusters A, B, and C are

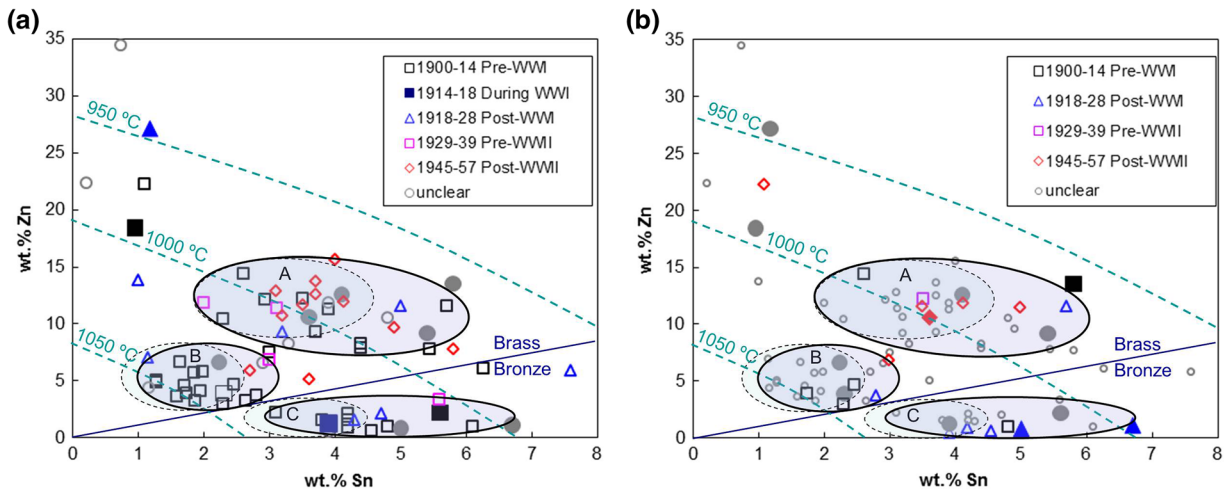


Fig. 6. Elemental composition plots (Zn versus Sn as determined by XRF) for sculptures identified by (a) date of sculpture creation and (b) casting date. The open symbols are from the current XRF data, which correlate with previous ICP-OES data,¹⁰ whereas the solid symbols are from the current XRF data from the 12 sculptures not previously reported. The three ovals indicate alloy clusters (A, B, and C) from the previous ICP-OES study¹⁰ (dashed lines) and the current XRF study (solid lines).

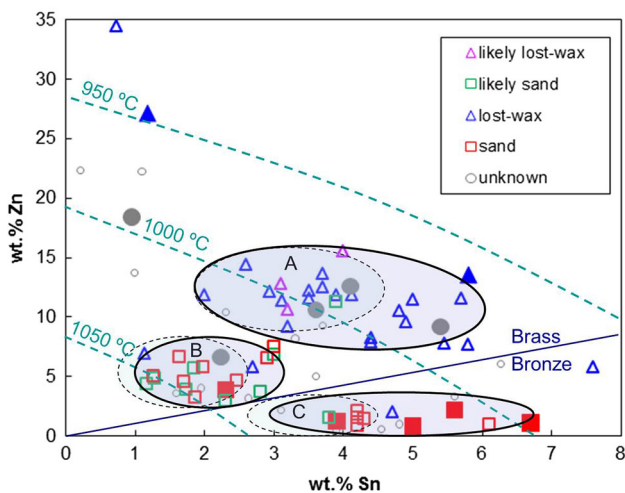


Fig. 7. Elemental composition plots (Zn versus Sn as determined by XRF) for sculptures identified by casting method. The open symbols are from the current XRF data, which correlate with previous ICP-OES data,¹⁰ whereas the solid symbols are from the current XRF data from the 12 sculptures not previously reported. The three ovals indicate alloy clusters (A, B, and C) from the previous ICP-OES study¹⁰ (dashed lines) and the current XRF study (solid lines).

represented by redefined A–C cluster ovals (ovals with solid lines in Figs. 4, 5, 6, and 7).

Composition Clusters

We focus here on the addition of the 12 new sculptures within the clusters identified previously from the original 62 sculptures.¹⁰ Of these 12 new sculptures, four fall in cluster A, two in cluster B, and four in cluster C, and two are outliers. It should be noted that, in an art historical context, all sculptures are referred to as “bronzes,” whereas, in a metallurgical context, alloys with higher Zn than

Sn concentrations are typically referred to as “brasses” and alloys with higher Sn than Zn concentrations are referred to as “bronzes.”

High-Zinc Brass (Cluster A) Brancusi’s Sleeping Muse (1931.523) with 13.6 wt.%Zn and 5.8 wt.%Sn falls near the edge of cluster A. It is known that it was lost-wax cast at the Valsuani foundry like the two previously reported Brancusi’s sculptures,¹⁰ *Danaide* (1967.30.6) and *Suffering* (1985.542). The new sculpture is just on the edge of cluster A and right next to *Danaide* in composition (11.6 wt.%Zn and 5.7 wt.%Sn).

Degas’ Rearing Horse (PMA: 1950.92.39) with 9.2 wt.%Zn and 5.4 wt.%Sn falls just on the edge of cluster A and is similar in composition to the two previously reported Degas sculptures,¹⁰ *Woman Rubbing Her Back with a Sponge, Torso* (PMA: 1954.92.21) and *Woman Taken Unawares* (PMA: 1963.181.82), which also fall on the high-Sn border of cluster A. Like Bernard’s *Girl with Pail* (AIC: 1943.1189) which is also in cluster A,¹⁰ all three Degas sculptures bear the mark of the lost-wax casting foundry of A.A. Hébrard. With a creation date of post-1920, *Degas’ Rearing Horse* further supports that this foundry, which operated from 1902 to 1936,²⁵ used the same metal composition many years beyond World War I.

Duchamp-Villon’s Portrait of Dr. Gosset (1963.371) with 10.2 wt.%Zn and 3.6 wt.%Sn falls into cluster A but is compositionally very different from his previous sculpture *Horse* (1957.165), which is an outlier with a very high Zn content (22.2 wt.%) and low Sn content (1.09 wt.%)¹⁰ and is the only sculpture reported from the Susse foundry. Falling into cluster A, *Duchamp-Villon’s Portrait of Dr. Gosset* (1963.371) composition is very different from castings from the Alexis Rudier foundry that fall

into cluster C. Since this is the first and only sculpture cast at the Georges Rudier foundry presented in this study, it is not possible to determine whether this composition is representative or unique to the Georges Rudier foundry.

Considering that the Hébrard foundry closed in 1936,²⁵ the late creation date of 1957 and its composition suggests that Duchamp-Villon's *Portrait of Dr. Gosset* was lost-wax cast at the Valsuani foundry, but it cannot be ruled out that another foundry was using an alloy of a similar composition.

Picasso's *Standing Woman 8* (1967.684) with a composition of 12.6 wt.%Zn and 4.1 wt.%Sn falls into cluster A and was most likely lost-wax cast between 1945 and 1947 at the Valsuani foundry, just like Picasso's previous seven sculptures from the same series, *Standing Woman 1–7*.¹⁰

Low-Zinc Alloys: Low-Tin Brass (Cluster B) Derain's *Man with Large Ears* (1978.410), with a composition of 6.63 wt.%Zn and 2.23 wt.%Sn, falls into cluster B, is the first Derain's sculpture to be reported compositionally as this artist was not reported in the previous ICP-OES study.¹⁰ It is difficult to determine its casting origins without further sculptures from the same artist. The compositional data here suggests that it could have been cast at the Bingen, Godard, or Valsuani foundry.

With a creation date of pre-1907, Poupelet's *Woman at Her Toilet* (1925.726), with a composition of 3.9 wt.%Zn and 2.3 wt.%Sn, also falls into cluster B. Like five of Poupelet's previous sculptures,¹⁰ most of these are known to have been sand cast between 1900 and 1910 or pre-1931. The compositional data here suggests that it would have been sand cast at the Godard or Bingen foundry, assuming another foundry was not using an alloy of similar composition.

Low-Zinc Alloys: Tin Bronze (Cluster C) Darde's sculpture, *Sorrow* (1950.143), falls into cluster C with 3.9 wt.%Sn and a low Zn content of 1.25 wt.%. No sculpture from this artist was studied in the previous study,¹⁰ so comparisons cannot be made. *Sorrow*, created in 1916 and bearing a Rudier foundry mark, was sand cast at the Alexis Rudier foundry and correlates with all other Rudier castings found in cluster C.

Known to have been created around 1909 and sand cast at the Rudier foundry, Maillol's *Enchained Action* (1955.29) is well within cluster C with 5.6 wt.%Sn and 2.2 wt.%Zn. Bearing a Rudier foundry mark, it is believed to be from the Alexis Rudier foundry; however, during this period, the foundry was run by Eugene Rudier.²⁵

With a composition of 5 wt.%Sn and 0.83 wt.%Zn, Rodin's *The Thinker* (RM: 1929.7.123) falls into cluster C like the previously studied sculptures by Rodin: *The Athlete* (PMA: 1967.30.73)¹⁰ and *The Athlete* (PMA: 1929.7.4).¹⁰ Rodin's second new sculpture, *Gates of Hell* (RM: 1929.7.128) with a composition of 6.7 wt.%Sn and 1.13 wt.%Zn,

because it is very rich in Sn, is located at the edge of cluster C. Like *The Athlete* (PMA: 1929.7.4), Rodin's new sculptures (*The Thinker* and *Gates of Hell*) both are known to have been cast at the Rudier foundry, further supporting the conclusion that this foundry used alloys of the same composition (very low Zn content) for a relatively long time frame, from 1904 to 1928. This finding is also supported by previous compositional studies on six Rodin²⁰ and one Laurier²¹ sculptures cast at the Rudier foundry.

Outliers Unlike the other foundries, Grandhomme-Andro, Hébrard, L. Gatti, Siot-Decauville, and Susse foundries have compositions with very high Zn content (13.7–34.4 wt.%) and very low Sn content (0.21–1.17 wt.%), which is essentially pure brass in composition compared with all other sculptures in this study.

Created between 1919 and 1920 and cast using the lost-wax method, Brancusi's *Golden Bird* (1990.88) has a very high Zn content (27.1 wt.%) and a very low Sn content (1.2 wt.%), which is compositionally unlike his other three sculptures previously studied,¹⁰ *Sleeping Muse* (1931.523), *Danaide* (1967.30.6), and *Suffering* (1985.542), which were all lost-wax cast at the Rudier foundry. This suggests that *Golden Bird* was cast elsewhere, based on the other data, it was possibly cast at the Grandhomme-Andro, Hébrard, L. Gatti, Siot-Decauville, or Susse foundries. However, it is also possible that Brancusi specifically requested a unique alloy composition; as the title suggests, the sculpture has a golden appearance in color, has no patina, and is highly polished.

Drappier's *Stray Horse* (1984.164) has a high Zn content of 18.4 wt.% and a low Sn content of 0.95 wt.%, placing it as an outlier. Created in 1906, *Stray Horse* is the first sculpture studied here and previously¹⁰ to be known to have been cast in the Siot-Decauville and the first by Drappier. According to Lebon,²⁵ Siot originally sand cast sculptures and only started lost wax casting in 1914. Unfortunately here, the casting date is unknown and would have been after 1906, so both casting methods are possible.

CONCLUSION

In this article, a comparison between previously collected ICP-OES measurements¹⁰ and newly reported XRF measurements is made for 62 modern bronze cast sculptures from the AIC and the PMA. There is good correlation between the two methods for the base metal (Cu), the two majority alloying elements (Zn and Sn), the minority alloying element (Pb), and the main impurity element (Fe). Thus, clusters related to the artist, foundry, casting date, and casting method—consisting of (A) high-zinc brass, (B) low-zinc alloys, low-tin brass, and (C) low-zinc, tin bronze—remain discernable independently of the analysis method used. This confirms that the XRF method, which is much more rapid than

ICP-OES and nondestructive (unlike ICP-OES), can be used effectively to help determine a sculpture's artist, foundry, date of creation, date of casting, and casting method, due to the reasonably large compositional variation between the three clusters, in concert with other scientific and art-historical methods.

The study was expanded by examining the XRF composition of 12 additional modern bronzes by Brancusi, Darde, Derain, Drappier, Duchamp-Villon, Picasso, Poupelet (from the AIC), Degas (from the PMA), and Rodin (from the RM). All but two (by Brancusi and Drappier) of these additional bronze sculptures fall in the previous clusters and further support the trends observed previously. Both outliers have very high Zn content and are nearly pure brass: (i) Drappier's *Stray Horse* (1984.164), which is the first casting from the Siot-Decauville foundry to be reported in our study here and previously,¹⁰ and (ii) Brancusi's *Golden Bird* (1990.88), which is unique because of its very highly polished surface and lack of patina providing the golden color from the casting title. Thus, a specific alloy (or at least color) might have been requested by Brancusi because the polished metal surface was meant to be seen for this sculpture.

ACKNOWLEDGEMENT

This research benefited from the financial support of the Andrew W. Mellon Foundation. The authors thank Francesca Casadio and Suzanne Schnepf (Art Institute of Chicago) for significant contributions to this article and useful discussions, Aniko Bezur (Institute for the Preservation of Cultural Heritage at Yale University) for useful discussions, Andrew Lins and Melissa Meighan (Philadelphia Museum of Art and Rodin Museum) for providing access to sculptures for XRF and ICP-OES measurements, and Juris Sarins (SIPI Metals Corporation) and Phil Meehan (National Bronze and Metals, Inc.) for providing bronze and brass reference materials.

REFERENCES

1. L. Dussubieux, *Restaura* 5, 328 (2007).
2. L. Dussubieux, *Archaeological Chemistry: Analytical Techniques and Archaeological Interpretation*, ed. M.D. Glascock, R.J. Speakman, and R.S. Popelka-Filcoff (Washington: American Chemical Society, 2007), pp. 336–348.
3. D. Bourgarit and B. Mille, *Meas. Sci. Tech.* 14, 1538 (2003).
4. A. Giunlia-Mair, E.J. Keall, A.N. Shugar, and S. Stock, *J. Archaeol. Sci.* 29, 195 (2002).
5. A. Giunlia-Mair, E.J. Keall, S. Stock, and A.N. Shugar, *J. Cult. Heritage* 1, 35 (2000).
6. I. Segal, A. Kloner, and I.B. Brenner, *J. Anal. At. Spectrom.* 9, 737 (1994).
7. I. Segal and S.A. Rosen, *Inst. Archaeo. Metall. Stud.* 25, 3 (2005).
8. R.H. Tykot and S.M.M. Young, *Archaeological Chemistry: Organic, Inorganic, and Biochemical Analysis*, ed. M.V. OrnaACS Symposium Series 625, (Washington: American Chemical Society, 1996), pp. 116–130.
9. S.M.M. Young, P. Budd, R. Haggerty, and A.M. Pollard, *Archaeometry* 39, 379 (1997).
10. M.L. Young, S. Schnepf, F. Casadio, A. Lins, M. Meighan, J.B. Lambert, and D.C. Dunand, *Anal. Bioanal. Chem.* 395, 171 (2009).
11. A.N. Shugar and J.L. Mass, *Handheld XRF for Art and Archaeology* Studies in Archaeological Sciences, (Leuven: Leuven University Press, 2012), pp. 1–473.
12. D. Kosinski, A. Boulton, S. Nash, and O. Shell, *Matisse: Painter as Sculptor* (New Haven: Yale University Press, 2007), pp. 1–312.
13. B.B. Considine, *Conserving Outdoor Sculpture: The Stark Collection at the Getty Center* (Los Angeles: Getty Conservation Institute, 2010), pp. 1–266.
14. H. Bronk, S. Rohrs, A. Bjeoumikhov, N. Langhoff, J. Schmalz, R. Wedell, H.E. Gorny, A. Herold, and U. Waldschlager, *Fresenius J. Anal. Chem.* 371, 307 (2001).
15. M. Ganio, A. Leonard, J. Slavant Plisson, and M. Walton (Paper presented at the ICOMOS Conference Métal à Ciel Ouvert. La Sculpture Metallique d'Exterieur du XIXe au Debut du XXe Siecle, Paris, France, 2014), pp. 136–145.
16. K. Uhler, M. Griesser, G. Buzanich, P. Wobruschek, C. Strelti, D. Wegryzynek, A. Markowicz, and E. Chinea-Cano, *X-Ray Spectrom.* 37, 450 (2008).
17. D.A. Scott, *Copper and Bronze in Art: Corrosion, Colorants, and Conservation* (Los Angeles: Getty Publications, 2002), pp. 1–534.
18. D.A. Scott, *Metallography and Microstructure in Ancient and Historic Metals* (Singapore: J. Paul Getty Museum, 1991), pp. 1–185.
19. M.L. Young, F. Casadio, J. Marvin, W.T. Chase, and D.C. Dunand, *Archaeometry* 52, 1015 (2009).
20. L. Robbiola and L.-P. Hurtel, *Mém. Études Scientif. Rev. Métall.* 12, 809 (1991).
21. L.S. Selwyn, N.E. Binnie, J. Poitras, M.E. Laver, and D.A. Downham, *Stud. Conserv.* 205, 205 (1996).
22. A. Adriaens, *Spectrochim. Acta Part B* 60, 1503 (2005).
23. D. Smith, *Studies in Archaeological Sciences: Handheld XRF for Art and Archaeology*, ed. A.N. Shugar and J.L. Mass (Leuven: Leuven University Press, 2012), pp. 37–74.
24. A. Heginbotham, A. Bezur, M. Bouchard, J.M. Davis, K. Eremin, J.H. Frantz, L. Glinsman, L.-A. Hayek, D. Hook, V. Kantarelou, A.G. Karydas, L. Lee, J. Mass, C. Matsen, B. McCarthey, M. McGath, A. Shugar, J. Sirois, D. Smith, and R.o.J. Speakman (Paper presented at Metal 2010. Proceedings of the International Conference on Metal Conservation, Charleston, SC, 2010), pp. 244–255.
25. É. Lebon, *Dictionnaire des Fondateurs de Bronze d'Art: France 1890–1950* (Perth: Marjon Editions, 2003), pp. 1–291.